High-excitation photoluminescence in GaN: Hot-carrier effects and the Mott transition

F. Binet and J. Y. Duboz
Laboratoire Central de Recherches, THOMSON-CSF, Domaine de Corbeville, 91404 Orsay Cedex, France

J. Off and F. Scholz
4, Physikalisches Institut, Universität Stuttgart, D-70550 Stuttgart, Germany
(Received 14 September 1998; revised manuscript received 11 January 1999)

Photoluminescence under intense excitation is studied in GaN. As the excitation density increases, we show the Mott transition between an excitonic recombination to a plasma-type recombination. The carrier density at the Mott transition is given. At and above the Mott density, we show that the carrier temperature is higher than the lattice temperature. The energy relaxation of the hot plasma is shown to be dominated by LO-phonon emission. Coulomb screening and band-gap renormalization are observed from the photoluminescence peak position and the measured renormalization factor is in good agreement with elementary many-body theory. Finally the dependence of the Mott density on carrier temperature is shown to follow a Debye-Hückel model. [S0163-1829(99)10727-6]

I. INTRODUCTION

The knowledge of physics in a semiconductor in a high injection regime is of particular importance when related to high-injection devices. This physics is now well established for GaAs and understood for the II-VI compounds like CdS and CdSe. This domain can be investigated by high-excitation photoluminescence. This was done, for instance, by Tanaka in GaAs (Ref. 1) and by Guillaume in CdS.[2] Whereas a hot-electron-hole plasma is created in GaAs at low lattice temperature and high density, the situation is different for CdS and turns out to be dominated by excitonic recombinations. Further studies showed that these conclusions were dependent on the injected carrier density and the excitation energy of the optical source.[3,4] This question is raised again with the emergence of gallium nitride and is of the highest interest as this compound is nowadays the best candidate for the realization of a blue laser.[5] Many studies have been dedicated to stimulated emission in optically pumped GaN and the resulting optical gain.[6–8] Stimulated emission brings, in fact, valuable information on the gain and the transparency threshold. However, as far as carrier recombination is concerned, a photoluminescence experiment is preferred as the spectrum is not affected by the optical amplification in the layer and is thus easier to interpret. In this study we propose an investigation of the optical properties of GaN under high optical injection. Section II deals with the experimental procedure employed for obtaining the high excitation photoluminescence spectra. These spectra are presented in Sec. III with their main features. Section IV deals with hot-carrier effects which can be extracted from the spectra. Section V emphasizes the renormalization process in GaN and its consequence on the photoluminescence spectra. We have observed the Mott transition in two ways: first, by the transition from (free or bound) exciton recombination at low excitation density, to free-electron/free-hole recombination within an electron-hole plasma at high-excitation density (above $\sim 3.8\times 10^{18}\,\mathrm{cm}^{-3}$); second, by the presence of hot carriers in the electron-hole plasma above the Mott transition.

II. EXPERIMENTAL PROCEDURE

The sample used in this study is a 2-μm-thick GaN film grown by a metal-organic chemical-vapor deposition (MOCVD) on a sapphire substrate. A nonintentional *n*-type doping of $3\times 10^{17}\,\mathrm{cm}^{-3}$ at 300 K was measured by the Hall effect. The full width at half maximum (FWHM) of the x-ray diffraction peak is 157 arc sec. The overall crystallographic quality is typical of what is obtained in such GaN layers. The photoluminescence experiment uses a quadrupled YAG (yttrium aluminum garnet) laser emitting at 4.66 eV with a pulse width of 20 ns and a repetition rate of 20 Hz. The pulse width of the laser is larger than the typical relaxation time in GaN (<1 ns) (Ref. 9): we can consider that steady state is reached during the pulses. The energy can be varied from 0 to 2 mJ per pulse. The incident beam is focused normally on the sample and the spontaneous emission is also normally collected and measured with an optical multichannel analyzer. This geometry avoids any distortion of the spontaneous spectrum by a parasitic effect of stimulated emission. A 5-mW He-Cd cw laser (3.81 eV) can be added to the experimental setup, allowing the measurement of a low power spectrum. The beam geometry is carefully analyzed and the incident power is measured with a power meter: the incident power density is thus determined. The GaN absorption coefficient has been carefully measured by the following method: we have thinned a part of the sample to different thicknesses by reactive ion etching and measured the optical transmission as a function of the GaN thickness. The exponential dependence gave us an absorption coefficient equal to $1.5\times 10^{5}\,\mathrm{cm}^{-1}$ at an energy of 4.66 eV and at low power density. Given the large difference between the excitation energy (4.66 eV) and the band-gap energy of gallium nitride (3.45 eV), any effect of stimulated emission on the absorption of the pump can be neglected. This absorption coefficient corresponds to an absorption length of 0.067 μm. A

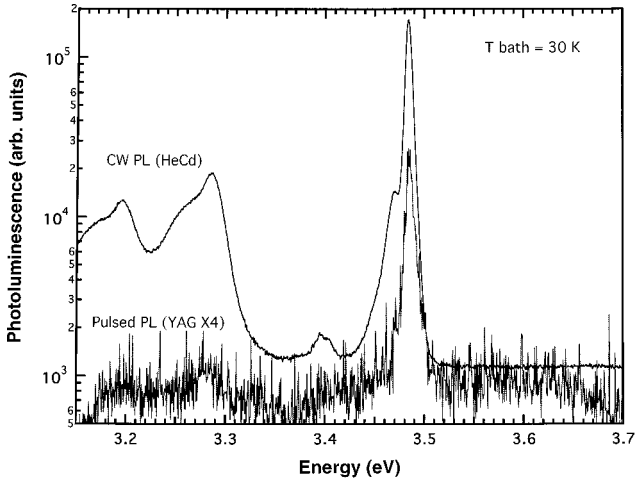

FIG. 1. Luminescence spectra of the GaN sample for a bath temperature of 30 K. One spectrum is obtained with a 5-mW cw He-Cd laser (3.81 eV). The other spectrum is measured with a 4 $\times$YAG laser (4.66 eV) with a very low incident power density.

diffusion length of about 0.1 μm has been measured in GaN by various techniques.[10] We thus take an effective absorption length d of 0.1 μm (effective absorption coefficient of $10^5\,\mathrm{cm}^{-1}$) to take the diffusion into account. The generation rate is then equal to the product of the absorption coefficient and the incident flux. In the case of an electron-hole plasma, the number of carriers optically injected in the sample can be deduced. The radiative recombination coefficient B has been determined from previous studies[11,12] to be equal to $1.3\times10^{-8}\,\mathrm{cm}^3\,\mathrm{s}^{-1}$. In this experiment, the incident power density is varied from 0.06 to 16 MW/cm^2, and the injected carrier density thus ranges from 7.4×10^{17} to $1.2\times10^{19}\,\mathrm{cm}^{-3}$.

III. EXPERIMENTAL LUMINESCENCE

The spectra obtained in this experiment are presented in logarithmic scale in Figs. 1 and 2 for a bath temperature of 30 K. The spectrum obtained with a cw He-Cd laser as the excitation source (3.81 eV) is shown in Fig. 1. It is dominated by an excitonic peak centered at 3.484 eV, attributed to the exciton bound to a neutral donor (D_0X). The free exciton (A exciton) peak can be seen (when the spectrum is plotted in linear scale) as a shoulder located about 6 meV above the bound exciton peak. For increasing temperatures (not presented here), the free exciton peak increases relative to the bound exciton peak and finally takes over for temperatures larger than 120 K. This spectrum can be compared with the spectrum obtained with the quadrupled YAG laser at low power (carrier density equal to several $10^{17}\,\mathrm{cm}^{-3}$). They are similar. The only difference is the degraded signal-to-noise ratio due to the small repetition rate (20 Hz) of the YAG laser. The spectra obtained with the quadrupled YAG laser and for increasing pumping power densities are shown in Fig. 2. Some of these spectra are labeled with their corresponding injected carrier density. With increasing density, the high-energy part of the spectrum takes on an exponential dependence on energy: at the highest power density, this high-energy tail extends from 3.5 to 3.6 eV. Moreover, the amplitude of the tail increases almost exponentially when the carrier density is above $3\times10^{18}\,\mathrm{cm}^{-3}$. This feature is the signature of hot-carrier effects. On the low-energy side, the spectrum broadens as the power density is increased. Several structures, almost periodic, appear below the main peak. They will be identified in the following as phonon replicas of a hot plasma. The main peak of the luminescence spectra redshifts with increasing carrier density, as shown in Fig. 2: this behavior will be described in terms of band-gap renormalization. The analysis of the shift of the peak will lead to the characterization of the Mott transition. The description of this transition with the Debye-Hückel model will be presented in Sec. V.

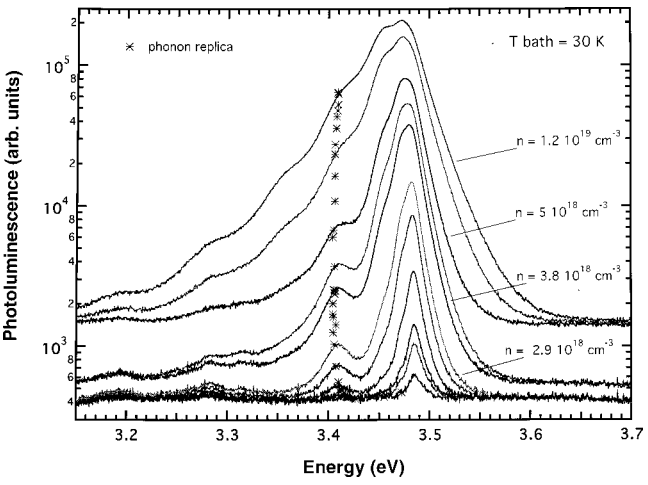

FIG. 2. Luminescence spectra of the GaN sample for a bath temperature of 30 K measured with a pulsed 4$\times$YAG laser (4.66 eV) with increasing incident power densities. Some of these spectra are labeled with the corresponding injected carrier density.

IV. HOT-CARRIER EFFECTS

The spontaneous-emission spectrum $I(h\nu)$ for band-to-band recombinations is proportional to the product of the electron and hole distribution functions, that is $I \propto f_c(E_e) f_v(E_h)$, where f_c and f_v are the Fermi-Dirac distributions and we have $h\nu = E_g + E_e + E_h$. If E_e and E_h are well above their quasi-Fermi energies and if the distributions are Maxwellian, then the product simplifies to

$$f_e(E_c) f_v(E_h) \propto e^{-E_c/kT_e} e^{-E_h/kT_e} = e^{-(h\nu - E_g)/kT_e}. \quad (1)$$

We assume here that the carrier temperature T_e is equal for electrons and holes.[4] Figure 3 presents a semilogarithmic plot of the high-energy part of the luminescence spectra obtained with the quadrupled YAG laser, for increasing incident power densities. At low incident power density, below 0.4 MW/cm^2 corresponding to a carrier density of $1.8\times10^{18}\,\mathrm{cm}^{-3}$, the high-energy tail is not perfectly exponential: the carrier temperature cannot be defined. Above 0.4 MW/cm^2, the tail is exponential over about one decade. In GaAs, the linear domain is found to be larger than two decades.[13] The smaller linear region in GaN can be explained by different factors. First, the plot is linear within 30–40 meV in both cases, and the smaller slope (due to the higher temperature) in our experiment reduces the signal dynamics. Second, GaAs and GaN have a different valence-band struc-

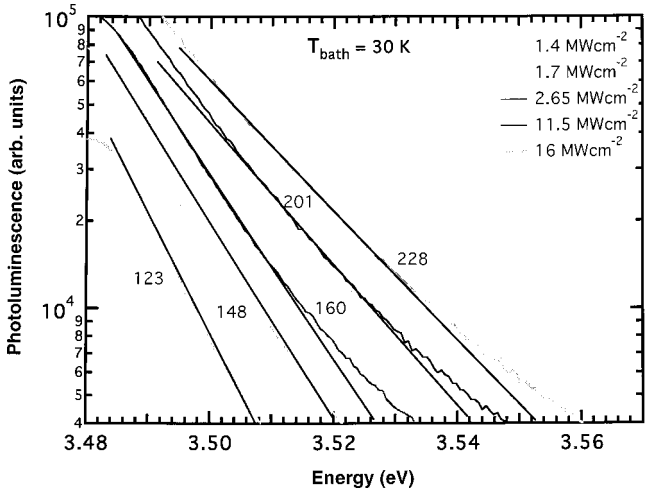

FIG. 3. Semilogarithmic plot of the high-energy tail of the luminescence spectra for different power densities. The exponential behavior of the tail allows the determination of the carrier temperature added in the figure.

ture. In GaAs, two of the valence bands are exactly degenerate at $k=0$ and the third valence band is split off by 340 meV due to the spin-orbit coupling; in hexagonal GaN, all three valence bands are split by the crystal field and the spin-orbit coupling. However, the splitting energies are small: in this the GaN layer grown on compression on sapphire, the energies between *A* and *B* excitons and between *B* and *C* excitons are about 10 and 20 meV, respectively.[14] Thus, one may expect some deviations from the simple theory (based on a single valence-band maximum) on the high-energy side of the photoluminescence tail in GaN. From Fig. 1, the carrier temperature is deduced for each power density by Eq. (1). For example, at 1.7 MW/cm^2, the carrier temperature deduced from the slope is equal to 148 K and is considerably larger than the bath temperature maintained at 30 K, thus proving the presence of a hot-carrier population. Moreover, the carrier temperature increases with the incident power density. We now proceed to explain the carrier-temperature dependence on the pumping power by considering the precise mechanisms of relaxation in the semiconductor.[4,13] In fact, the illumination of the GaN sample (band-gap energy $E_g \approx 3.48$ eV) with the YAG laser ($E=4.66$ eV) creates carriers in their respective bands with an excess energy ΔE_i given by $\Delta E_i = m_r/m_i\ (E-E_g)$, where m_r is the reduced mass, m_i is the *i* carrier mass ($i=e,h$) and we neglect here the band nonparabolicity. The hole mass ($0.8m_0$) (Ref. 15) being larger than that of the electron ($0.22m_0$),[15] the excess energy given to the electron (925 meV) is far larger than the one given to the hole (254 meV): as a first simplification, we will only consider the electron population.

The photoexcited electron is then located high in the tail of the distribution function. The other electrons located at the bottom of the conduction band are in quasiequilibrium and form the electron gas. There are mainly two relaxation paths for the very energetic electron:[13] either an interaction with the lattice through phonon emission or a direct collision with the electron gas (e-e).

Regarding the electron-lattice interaction, acoustic-phonon emission can be ruled out since the excess energy to be relaxed (935 meV) is very important.[4] The efficient mechanism is therefore rather an emission of longitudinal-optical (LO) phonons, the energy of a LO phonon in GaN being as large as $E_{\mathrm{LO}}=92$ meV.[15] The photoexcited electron can cool down towards the electron gas by emitting up to 10 LO phonons since $\Delta E_e = 935\,\mathrm{meV} = 10E_{\mathrm{LO}} + \delta E$. The residual of energy δE, equal here to 5 meV can be relaxed by two mechanisms: either acoustic-phonon emission or the interaction with the electron gas. Note that only the latter mechanism transfers energy to the electron gas. The energy dissipation rate through LO-phonon emission $(d\varepsilon/dt)_{e\text{-LO}}$ is deduced from the probability for an electron to emit or absorb a LO-phonon and is independent of the carrier density[13]

$$\left(\frac{d\varepsilon}{dt}\right)_{c\text{-LO}} = \frac{2eE_0E_{\mathrm{LO}}}{(2m_e\varepsilon)^{1/2}}\left[N_q \sinh^{-1}\left(\frac{\varepsilon}{E_{\mathrm{LO}}}\right)^{1/2} - (N_q+1)\sinh^{-1}\left(\frac{\varepsilon - E_{\mathrm{LO}}}{E_{\mathrm{LO}}}\right)^{1/2}\right], \tag{2}$$

where ε is the energy of the photoexcited electron, N_q is the occupation number of phonons of wave vector q interacting with the electron; given the fact that the LO-phonon energy in GaN is far larger than the thermal energy up to room temperature, it should be noted that N_q is much smaller than unity: the bath temperature dependence of $(d\varepsilon/dt)_{e\text{-LO}}$ can be neglected. E_0 is an effective field given by

$$eE_0 = \frac{m_e e^2 E_{\mathrm{LO}}}{4\pi\hbar^2\varepsilon_0}\left(\frac{1}{K_\infty} - \frac{1}{K_0}\right), \tag{3}$$

where ε_0 is the free-space permittivity, K_∞ and K_0 are the optical and the static dielectric constants, respectively, equal to 5.2 and 9.6.[16] In GaN, (eE_0) is found equal to 0.33 MeV/cm.

The second path of relaxation for the photoexcited electron is a direct interaction with the electron gas through electron-electron collisions. The energy dissipation rate through electron-electron collisions $(d\varepsilon/dt)_{e\text{-}e}$ can be written by analogy with metals[13]

$$\left(\frac{d\varepsilon}{dt}\right)_{e\text{-}e} = \frac{-ne^4}{4\pi K^2 (2m_e\varepsilon)^{1/2}\varepsilon_0^2}, \tag{4}$$

where n is the carrier density and K is the average dielectric function. One has to estimate the relative importance of electron-electron collisions compared to LO-phonon emission. The theoretical work and the experimental approach have been well described by Shah and will be applied here for GaN.[13] The two dissipation rates are equal if the carrier density is equal to a critical density n_c^* given by[13]

$$n_c^* = \frac{8\pi e E_0 E_{\mathrm{LO}} K^2 \varepsilon_0^2}{e^4}\left[(N_q+1)\sinh^{-1}\left(\frac{\varepsilon - E_{\mathrm{LO}}}{E_{\mathrm{LO}}}\right)^{1/2} - N_q \sinh^{-1}\left(\frac{\varepsilon}{E_{\mathrm{LO}}}\right)^{1/2}\right]. \tag{5}$$

In the GaN case, for a bath temperature of 30 K, the value of n_c^* is found equal to $2.4\times10^{19}\,\mathrm{cm}^{-3}$. Hence for a carrier density far lower than n_c^*, the photoexcited electron relaxes primarily through LO-phonon emission. If $n \approx n_c^*$, both

mechanisms are considered and F is defined as the probability that a very energetic carrier is involved in an electron-electron collision. F is thus roughly equal to $n/(n+n_c^*)$. Given the experimental density range (7×10^{17}–$1.4\times10^{19}\,\mathrm{cm}^{-3}$) and the value of n_c^*, the electron-electron collision is never dominant and F varies from 0.004 to 0.375. The excess energy $F\Delta E_e$ given to the electron gas by the photoexcited electron through electron-electron collisions thus varies from 3.7 to 350 meV. Hence, for carrier densities larger than $10^{18}\,\mathrm{cm}^{-3}$, $F\Delta E_e$ is far larger than $\delta E = 5$ meV: the electron-gas heating is mainly due to the primary electron-electron collision.

If collisions between carriers in the electron gas are more frequent than phonon emissions, the electron gas can thermalize towards a Maxwell-Boltzmann distribution characterized by an electron temperature T_e. Averaging Eq. (2) over such a distribution gives the power $P(T_e)$ dissipated by the electron gas per photoexcited electron,[13]

$$P(T_e)=\frac{2E_{\mathrm{LO}}}{m_e}(eE_0)\left(\frac{e^{x_0-x_e}-1}{e^{x_0}-1}\right)\left[\frac{(x_e/2)^{1/2}e^{(x_e/2)}K_0(x_e/2)}{\sqrt{\pi/2}}\right], \tag{6}$$

where $x_0=E_{\mathrm{LO}}/T_L$ and $x_e=E_{\mathrm{LO}}/T_e$, T_L is the lattice temperature and K_0 is the modified, zero-order Bessel function. Let us come back now to the condition of thermalization: the thermalization within the gas (electron-electron collisions) has to occur more rapidly than the LO-phonon emission. This condition is obtained by comparing the electron-electron collision rate and the electron-phonon collision rate and is fullfilled when $n>n_c$, where[13]

$$n_c=(8\sqrt{\pi}/e^4)\hbar\omega_0K^2\varepsilon_0^2(eE_0)\left(\frac{e^{x_0-x_e}-1}{e^{x_0}-1}\right)e^{x_e/2}K_0(x_e/2). \tag{7}$$

In our case, for a carrier density in the range of 7×10^{17} to $1.4\times10^{19}\,\mathrm{cm}^{-3}$, n_c varies from 9×10^{14} to $5.3\times10^{16}\,\mathrm{cm}^{-3}$. The condition for internal thermalization is thus satisfied: T_e is defined. The experimental results indeed show a Maxwell-Boltzmann distribution for carrier densities above $1.8\times10^{18}\,\mathrm{cm}^{-3}$. However, for carrier densities lower than $1.8\times10^{18}\,\mathrm{cm}^3$, the bahavior of the tail is not exponential although $n>n_c$. This may be attributed to the existence of excitons at smaller densities, as will be discussed later in this paper.

The power P_{lum} given to the gas by the photoexcited electrons is[13]

$$P_{\mathrm{lum}}=(I/d)(W/E)(1/n), \tag{8}$$

where I is the incident power density, d is the effective absorption length, E is the photon energy, and $W=F\Delta E_e+\delta E$. In steady state, P_{lum} is equal to $P(T_e)$. In the case where the LO-phonon energy is much larger than the thermal lattice temperature kT_L and the electron thermal energy kT_e, the bracketed quantity in Eq. (6) reduces to unity and the balance equation becomes[13]

$$P(T_e)=\left(\frac{2E_{\mathrm{LO}}}{m^e}\right)^{1/2}(eE_0)\exp\left(-\frac{E_{\mathrm{LO}}}{kT_E}\right)=(I/d)(W/E)(1/n). \tag{9}$$

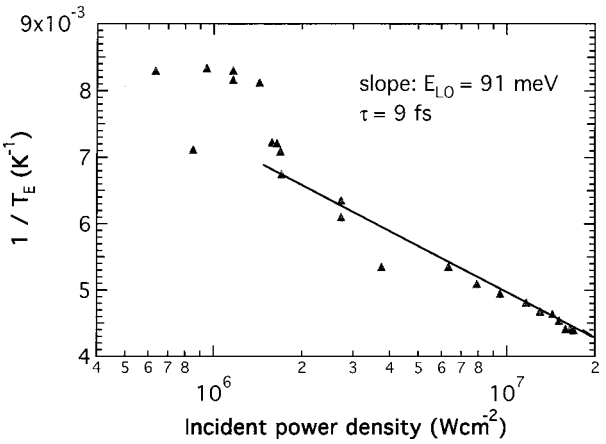

FIG. 4. Arrhenius plot of the carrier temperature T_e versus the incident power density. An Arrhenius behavior is obtained for power densities larger than 1.6 MW/cm^2. A linear fit allows the determination of the activation energy equal to the LO-phonon energy in GaN (91 meV). The study of the intercepts gives an effective relaxation time of 9 fs.

Hence, for sufficiently low lattice temperatures, the electron temperature follows an Arrhenius law and the activation energy is 92 meV.[15] $P(T_e)$ is usually written as follows:[4]

$$P(T_E)=\left(\frac{E_{\mathrm{LO}}}{\tau}\right)\exp\left(-\frac{E_{\mathrm{LO}}}{kT_E}\right). \tag{10}$$

The characteristic time τ takes into account the effective field (eE_0) and the LO-phonon energy E_{LO}. As exposed by Lyon, τ has no precise physical meaning since it is a complex function of all the characteristic physical times involved in the calculation.[4] For GaN, τ is evaluated to be 7 fs. Experimentally, for each power density, a carrier temperature is deduced from the high-energy tail of the photoluminescence spectrum. Figure 4 represents the Arrhenius plot of T_e as a function of the incident power density I. This plot shows data only for $I>0.4\,\mathrm{MW/cm}^2$, i.e., $n>1.8\times10^{18}\,\mathrm{cm}^{-3}$, where the electron temperature is defined. First from 0.4 to 1.6 MW/cm^2, the electron temperature remains almost constant and equal to 120 K: this particular behavior will be examined in the following. Above 1.6 MW/cm^2, the electron temperature increases and follows an Arrhenius behavior. The slope gives an activation energy equal to 9 meV. This result is consistent with the hot-carrier gas relaxation through LO-phonon emission. The intercept of the Arrhenius plot of Fig. 4 allows us to estimate τ equal to 9 fs. The agreement of the experimental luminescence results with the general theory of hot photoexcited carriers is thus good. From far-infrared polarized reflexion spectra performed on highly doped GaN samples ($3\times10^{19}\,\mathrm{cm}^{-3}$) at room temperature, Manchon *et al.* measured an electron relaxation time of 3.8 fs.[17] The scattering time of an electron by LO phonons (E_1 and A_1) was directly measured by time-resolved Raman diffusion.[18] The measured value of 25 fs is one order of magnitude smaller than in GaAs, which was explained in terms of the large ionicity of GaN. Although our effective time cannot be directly compared with scattering times measured by other methods, we can compare it with the value obtained by the

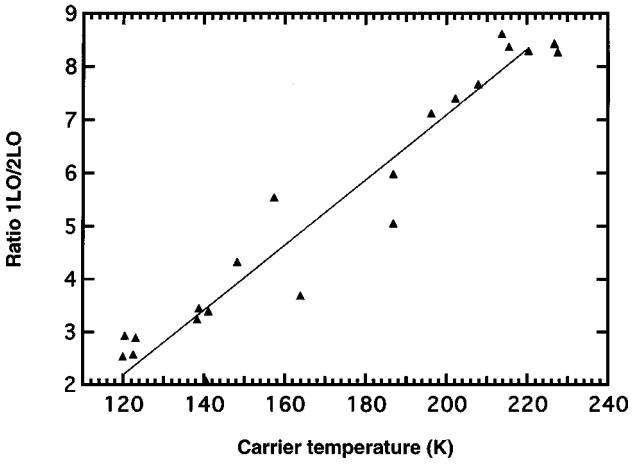

FIG. 5. Evolution of the amplitude ratio between the first and the second phonon replica as a function of the carrier temperature.

same method in GaAs. Values in the range of 100 fs to 1 ps are obtained in bulk or in GaAs quantum wells.[4] Whatever the measurement method is, the comparison with GaAs shows that electron–LO-phonon scattering times are shorter in GaN than in GaAs by a factor of 10 or more. It is thus expected that the LO-phonon emission is the main relaxation path for the hot electron population in GaN (Ref. 19) as it is the case in GaAs.[13] Our experiment has confirmed this point.

Let us now examine the low-energy part of the spectra of Fig. 2. Periodic structures are phonon replica. The first phonon replica, due to the non-k-conservation, is expected[20] at an energy $E_p^1 = E_g - E_{\mathrm{LO}} + 2kT_e$. The last term, usually negligible in a low-power luminescence experiment, is in this case very important. In fact, the carrier temperature is found to vary from 120 to 240 K with increasing pumping power, corresponding to a carrier thermal energy of 10.4 to 20.7 meV. The peak energy associated with the interband transition is expected[20] at $E_{\mathrm{peak}} = E_g + 0.5kT_e$. As a consequence, the first phonon replica is separated from the main peak by a quantity equal to $E_{\mathrm{LO}} - 1.5kT_e$, lower than the LO-phonon energy (92 meV). The theoretical position can be calculated for each power density (carrier temperature) and is represented in Fig. 2 (stars). The agreement between the calculated and the measured replica positions is very good. The following structures at even lower energy are periodically spaced with an energy separation of 92 meV. General theory of exciton-phonon coupling predicts that the spectral shape of a phonon replica is given by the product of $W_n(E_{\mathrm{ke}})$, the transition probability times the Maxwell-Boltzmann distribution function of the excitons, which depends on the carrier temperature and the kinetic energy E_{ke} of the excitons. It can be shown[21,22] that the probability $W(1\mathrm{LO})$ of one LO-phonon-assisted emission is proportional to the kinetic energy E_{ke} of the exciton, and the probability of a two LO-phonon-assisted emission is independent of E_{ke}. The amplitude ratio between the first and the second phonon replica is therefore proportional to the kinetic energy of the excitons, i.e., to the carrier temperature.[23] We will assume here that the general behavior of these phonon replicas is valid also for the hot electron-hole plasma since the distribution function of the plasma is Maxwellian. Figure 5 presents

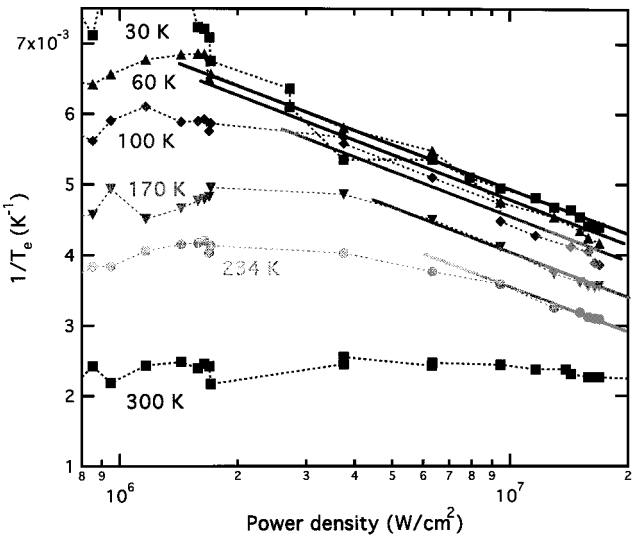

FIG. 6. Arrhenius plot of the carrier temperature T_e versus the incident power density for different bath temperatures. The E_{LO} slope has been added in the high-energy part of the curves.

the variation of this ratio with the carrier temperature, defined for power densities larger than 0.4 MW/cm^2. The behavior is, as expected, linear.

Similar experiments were performed for different bath temperatures. As was done for the case of $T_{\mathrm{bath}} = 30$ K, the carrier temperature was measured from the exponential high-energy tail as a function of the incident power density. Hot-carrier effects are also noticed for bath temperatures larger than 30 K. The Arrhenius plot of the carrier temperature as a function of the power density is presented in Fig. 6 for five different bath temperatures: {30, 60, 100, 170, 234, 300 K}. For sufficiently high power densities and for bath temperatures lower than 170 K, T_e follows an Arrhenius law with I and the activation energy E^* is around 92 meV, showing that the hot-carrier gas relaxes through LO-phonon emission. At 234 K, the slope value is 10 meV larger than E_{LO} and at 300 K, E^* equals 230 meV. The power density range where the Arrhenius plot is valid is also smaller when the lattice temperature is higher. These observations can be qualitatively described by the theoretical balance relation written in Eq. (9) but without the approximation to Eq. (6) that we made for the low-temperature case. Figure 7 plots this theoretical relation for the bath temperatures considered here. For bath temperatures lower than 100 K, all the curves coincide and the Arrhenius plot is valid. For a given power density, when the bath temperature increases above 100 K, the carrier temperature also increases but the difference between the carrier and the lattice temperature decreases. Furthermore, the power density range of validity of the Arrhenius plot is decreasing with lattice temperature. This behavior can be qualitatively understood by a stronger effect of the electron-phonon interaction at elevated bath temperatures. Thus all our observations are in good agreement with the hot-carrier theory.

V. BAND-GAP RENORMALIZATION AND MOTT DENSITY

From Fig. 2, a redshift of the main peak in the luminescence spectra can be noticed. Figure 8 plots the energetical

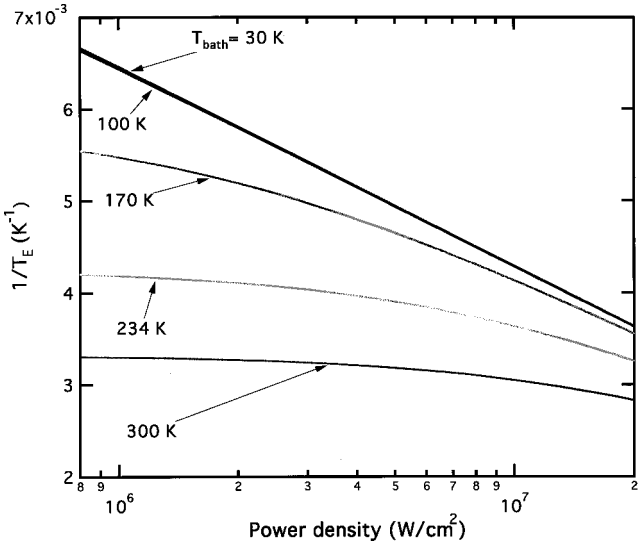

FIG. 7. Theoretical relation between the carrier temperature T_e and the incident power density for different bath temperatures. Parameters are $d=0.1\,\mu$m, $m_e=0.22$ m, $E_{\mathrm{LO}}=92$ meV, and $K=7.4$. Curves for a bath temperature of 30, 60, and 100 K cannot be distinguished.

position of this peak as a function of the cubic root of the carrier density at a bath temperature of 30 K. For carrier densities greater than $1.8\times10^{18}\,\mathrm{cm}^{-3}$, the peak redshifts linearly with the cubic root of the carrier density. This behavior is symptomatic of a band-gap renormalization.[24] A rough calculation of the band-gap renormalization performed to first order, taking into account the exchange energy only, predicts a lowering of the band-gap energy ΔE_g such as $\Delta E_g=-\alpha n^{1/3}$. α is known as the renormalization coefficient and depends only on the exciton energy of the material. For GaN, this calculation leads to a theoretical value for α equal to 1.5×10^{-8} eV cm. Such a renormalization does not depend on the carrier temperature if the plasmon energy is larger than the carrier thermal energy kT_e. When the carrier temperature T_e varies from 100 to 400 K, kT_e ranges from 8.6 to 34.5 meV. The corresponding range of carrier densities investigated in the experiment is $10^{18}-10^{19}\,\mathrm{cm}^{-3}$, giving an electron plasmon energy of 25 to 81 meV. In these conditions, the band-gap renormalization is thus independent of the carrier temperature. From studies performed on highly doped *n*-type GaN samples, a band-gap renormalization coefficient α equal to 2.1×10^{-8} eV cm[25] or 2.4×10^{-8} eV cm (Ref. 26) was found. If we take into account the thermal blueshift equal to $0.5kT_e$ (Ref. 20), a total shift equal to $\Delta E=-\alpha n^{1/3}+0.5kT_e$ is expected for the photoluminescence peak. In Fig. 8 the corresponding fit of the experimental shift is presented for carrier densities larger than $1.8\times10^{18}\,\mathrm{cm}^{-3}$. Let us recall that the carrier temperature can be deduced from the spectrum. The only parameters of the fit are thus the fundamental band-gap energy and the band-gap renormalization coefficient α. α found from the fit is equal to 2.1×10^{-8} eV cm, in very good agreement with the previous experimental results (Ref. 25), and in a pretty good agreement with our first-order theoretical calculation. The uncertainty of our determination can be estimated to be about 20%. At low carrier densities, $n<1.8\times10^{18}\,\mathrm{cm}^{-3}$, the peak remains located near $E=3.484$ eV. This position is exactly the energy of the excitonic peak, known from the photoluminescence spectra obtained at low power density with the He-Cd laser (3.81 eV). This is due to a compensation effect between the redshift produced by the band-gap renormalization and the blueshift induced by the screening of the Coulomb potential. Because of this screening, the exciton binding energy decreases with increasing carrier densities as $-\alpha n^{1/3}$ and finally vanishes at the Mott transition, for a carrier density of $1.8\times10^{18}\,\mathrm{cm}^{-3}$. A closer examination of the spectra (not presented here) in this density range indicates the following evolution. With increasing pump intensities, the peak attributed to the bound exciton remains at a constant energy while the free *A* exciton shoulder seems to redshift towards the bound exciton peak, the two peaks finally merging for a density around $1.8\times10^{18}\,\mathrm{cm}^{-3}$. (However, this shoulder is barely discernable and our data are not precise enough to allow us to investigate more deeply the roles of bound and free excitons in the Mott transition. This remains an open subject.) We consider that the Mott transition occurs between free excitons and free electron-hole pairs and we will use free-exciton parameters to describe it.

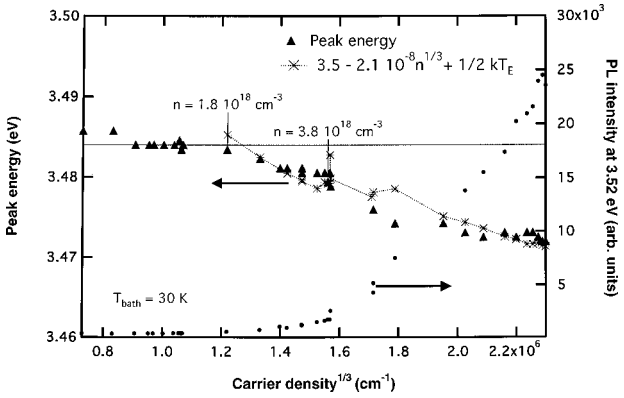

FIG. 8. Experimental position of the luminescence peak as a function of the cubic root of the density. The horizontal line represents the energy of the excitonic peak which is constant up to $1.8\times10^{18}\,\mathrm{cm}^{-3}$. Star points correspond to a model of renormalization, taking into account the carrier temperature. The amplitude of the photoluminescence at 3.52 eV is also represented (right axis): a threshold can be defined corresponding to a carrier density equal to $3.8\times10^{18}\,\mathrm{cm}^{-3}$.

As a result of the evolution of the exciton binding energy with the carrier density, we expect the formation of a hot electron-hole plasma for carrier densities larger than $1.8\times10^{18}\,\mathrm{cm}^{-3}$. However, we notice that between $1.8\times10^{18}\,\mathrm{cm}^{-3}$ and $3.8\times10^{18}\,\mathrm{cm}^{-3}$, the carrier temperature remains constant, equal to 120 K. This may be related to the coexistence of excitons and electron-hole pairs in this intermediate density range. In the same way, the amplitude of the photoluminescence signal at 3.52 eV (in the high-energy tail) is plotted in Fig. 8, as a function of the cubic root of the density. The amplitude rises drastically above a threshold here defined at $3.8\times10^{18}\,\mathrm{cm}^{-3}$. Hence, instead of a unique Mott density, we may define a Mott density range here equal to $1.8\times10^{18}-3.8\times10^{18}\,\mathrm{cm}^{-3}$ for a bath temperature of 30 K. In the following, only the higher limit will be considered as the Mott density n_M ($3.8\times10^{18}\,\mathrm{cm}^{-3}$). Such a density n_M has been identified for each bath temperature investigated in

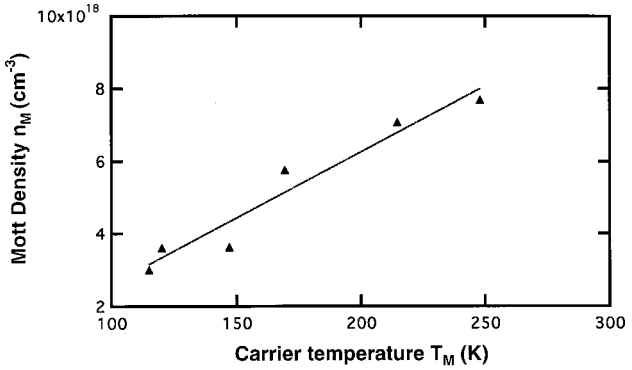

FIG. 9. Variation of the Mott density with its associated carrier temperature for different bath temperatures (30, 60, 100, 170, 234 K). The dashed line represents a linear fit of the curve.

this study: {30, 60, 100, 170, 234, 300} and associated with a measured carrier temperature T_M. Figure 9 plots the Mott density n_M as a function of T_M. n_M increases nearly linearly with T_M up to a bath temperature of 234 K. The couple of points (T_M, n_M) obtained for a bath temperature of 300 K deviates from this linear behavior and is not included in Fig. 9. The reason for this is not completely clear at the moment but could be related to the difficulty in identifing the Mott transition at 300 K. The slope of the linear fit equals $3.7 \times 10^{16}\,\mathrm{K}^{-1}\,\mathrm{cm}^{-3}$. In order to explain this behavior, we can assume that the plasma is described by classical Boltzmann statistics. In that case, the Mott density can be deduced from the Debye-Hückel model and is given by[23]

$$n_M = \frac{(1.19)^2 k T_M}{4 E_{ex} a_0^3}, \tag{11}$$

where E_{ex} is the exciton binding energy and a_0 is the excitonic Bohr radius. Taking a value of 25 meV for E_{ex} (Ref. 27) and a reduced mass equal to 0.17,[15] the theoretical coefficient of proportionality between n_M and T_M is $4.5 \times 10^{16}\,\mathrm{K}^{-1}\,\mathrm{cm}^{-3}$. The agreement with the experimental data is thus very satisfactory for bath temperatures up to 234 K.

VI. CONCLUSION

We have investigated hot-carrier effects in GaN. Theoretically, it is shown that in the range of 10^{18}–$10^{19}\,\mathrm{cm}^{-3}$ for the injected carrier density, the relaxation of a photoexcited carrier can occur through LO-phonon emission or collisions with the electron gas. In the case of GaN, the energetical contribution of the last mechanism to the gas is important and induces the formation of a hot plasma. The analysis of the high-energy tail of the luminescence spectra indicates that carriers are in a Maxwell-Boltzmann distribution with a carrier temperature larger than the lattice temperature. The experimental evolution of the carrier temperature with the power density shows that the main path of energy relaxation of the hot plasma is the LO-phonon emission. An effective relaxation time is deduced equal to 9 fs. The study of the relaxation of the hot plasma as a function of the lattice temperature shows that the carrier-lattice interaction plays a rising role for increasing lattice temperature. A pretty good agreement of the overall results is found with the hot carrier theory. On the low-energy part of the spectra, the LO-phonon replicas are identified and the analysis of their amplitudes confirms the Maxwellian nature of the plasma.

Band-gap renormalization has also been investigated: it is shown that the main luminescence peak follows the influence of both the band-gap renormalization and the effect of the carrier temperature. A band-gap renormalization coefficient is extracted from the experimental study, equal to $2.1 \times 10^{-8}\,\mathrm{eV\,cm}$, in good agreement with previous studies on GaN and a basic many-body theory. Below the Mott density ($2-3 \times 10^{18}\,\mathrm{cm}^{-3}$ at 30 K), carriers are described in terms of excitons rather than an electron-hole plasma. Below the Mott transition, the observed luminescence peak energy is independent of the pump intensity. We ascribe this lack of variation with pump intensity to the cancellation of two opposing effects: the redshift due to the band-gap renormalization, and the blueshift due to the screening of the electron-hole Coulomb potential. Both effects scale with $n^{1/3}$, where n is the carrier density. We have studied the Mott transition as a function of the bath temperature. We found that the carrier density and temperature at the Mott transition increase with the bath temperature. Moreover, the Mott carrier density increases linearly with the carrier temperature, following a Debye-Hückel model.

ACKNOWLEDGMENTS

The authors are grateful to B. Vinter for many helpful conversations concerning hot-carrier theory and band-gap renormalization. We thank B. Gil and M. Leroux for their critical reading of a first report of these results.

[1] S. Tanaka, H. Kobayashi, H. Saito, and S. Shionoya, J. Phys. Soc. Jpn. **49**, 1051 (1980).
[2] C. B. A. L. Guillaume, J. M. Debever, and F. Salivan, Phys. Rev. **177**, 567 (1969).
[3] F. A. Majumder, H. E. Swoboda, K. Kempf, and C. Klingshirn, Phys. Rev. B **32**, 2407 (1985).
[4] S. A. Lyon, J. Lumin. **35**, 121 (1986).
[5] S. Nakamura, M. Senoh, S. I. Nagahama, N. Iwasa, T. Yamada, T. Matsushita, Y. Sugimoto, and H. Kiyoku, Appl. Phys. Lett. **70**, 868 (1997).
[6] S. Kurai, Y. Naoi, T. Abe, S. Ohmi, and S. Sakai, Jpn. J. Appl. Phys., Part 2/1B **35**, L77 (1996).
[7] O. Gluschenkov, J. M. Myoung, K. H. Shim, K. Kim, Z. G. Figen, J. Gao, and J. G. Eden, Appl. Phys. Lett. **70**, 811 (1997).
[8] X. Zhang, P. Kung, A. Saxler, D. Walker, and M. Razeghi, J. Appl. Phys. **80**, 6544 (1996).
[9] J. S. Im, A. Moritz, F. Steuber, V. Härle, F. Scholz, and A. Hangleiter, Appl. Phys. Lett. **70**, 631 (1997).
[10] J. Y. Duboz, F. Binet, D. Dolfi, N. Laurent, F. Scholz, J. Off, A. Sohmer, O. Briot, and B. Gil, Mater. Sci. Eng., B **50**, 289 (1997).
[11] F. Binet, J. Y. Duboz, E. Rosencher, F. Scholz, and V. Härle, Appl. Phys. Lett. **69**, 1202 (1996).
[12] J. F. Muth, J. H. Lee, I. K. Smagin, R. M. Kolbas, H. C. Casey, B.

P. Keller, U. K. Mishra, and S. P. DenBaars, Appl. Phys. Lett. **71**, 2572 (1997).
[13] J. Shah, Solid-State Electron. **21**, 43 (1978).
[14] B. Gil, O. Briot, and R. L. Aulombart, Phys. Rev. B **52**, 17 028 (1995).
[15] D. K. Gaskill, L. B. Rowland, and K. Doverspike, *Properties of Group III Nitrides* (INSPEC Production, London, 1994).
[16] F. Demangeot, J. Frandon, M. A. Renucci, C. Meny, O. Briot, and R. L. Aulombard, J. Appl. Phys. **82**, 1305 (1997).
[17] D. D. Manchon, A. S. Barker, P. J. Dean, and R. B. Zetterstrom, Solid State Commun. **8**, 1227 (1970).
[18] K. T. Tsen, D. K. Ferry, A. Botchkarev, B. Sverdlov, A. Salvador, and H. Morkoç, Appl. Phys. Lett. **71**, 1852 (1997).
[19] S. J. Sheih, K. T. Tsen, D. K. Ferry, A. Botchkarev, B. Sverdlov, A. Salvador, and H. Morkoç, Appl. Phys. Lett. **67**, 1757 (1995).
[20] L. Pavesi and M. Guzzi, J. Appl. Phys. **75**, 4779 (1994).
[21] B. Monemar, I. A. Buyanova, J. P. Bergman, H. Amano, and I. Akasaki, Mater. Sci. Eng., B **43**, 172 (1997).
[22] D. Kovalev, B. Averboukh, D. Volm, B. K. Meyer, H. Amano, and I. Akasaki, Phys. Rev. B **54**, 2518 (1996).
[23] C. F. Klingshirn, *Semiconductor Optics* (Springer-Verlag, Berlin, 1997).
[24] H. Haug and S. W. Koch, Phys. Rev. A **39**, 1887 (1989).
[25] B. K. Meyer, D. Volm, A. Graber, H. C. Alt, T. Detchprohm, A. Amano, and I. Akasaki, Solid State Commun. **95**, 597 (1995).
[26] X. Zhang, S. J. Chua, W. Liu, and K. B. Chong, Appl. Phys. Lett. **72**, 1890 (1998).
[27] S. Chichibu, A. Shikanai, T. Azuhata, T. Sota, A. Kuramata, K. Horino, and S. Nakamura, Appl. Phys. Lett. **68**, 3766 (1996).